Massively Parallel Functional Analysis of BRCA1 RING Domain Variants

Lea M. Starita,* David L. Young,* Muhtadi Islam,[†] Jacob O. Kitzman,*[,1] Justin Gullingsrud,*
Ronald J. Hause,* Douglas M. Fowler,* Jeffrey D. Parvin,[†,2] Jay Shendure,*[,2] and Stanley Fields*[,‡,§,2]

*Department of Genome Sciences, ‡Department of Medicine, and §Howard Hughes Medical Institute, University of Washington,
Seattle, Washington 98195, and †Department of Biomedical Informatics and The Ohio State University Comprehensive Cancer
Center, The Ohio State University, Columbus, Ohio 43210

ABSTRACT Interpreting variants of uncertain significance (VUS) is a central challenge in medical genetics. One approach is to experimentally measure the functional consequences of VUS, but to date this approach has been *post hoc* and low throughput. Here we use massively parallel assays to measure the effects of nearly 2000 missense substitutions in the RING domain of BRCA1 on its E3 ubiquitin ligase activity and its binding to the BARD1 RING domain. From the resulting scores, we generate a model to predict the capacities of full-length BRCA1 variants to support homology-directed DNA repair, the essential role of BRCA1 in tumor suppression, and show that it outperforms widely used biological-effect prediction algorithms. We envision that massively parallel functional assays may facilitate the prospective interpretation of variants observed in clinical sequencing.

KEYWORDS deep mutational scanning; BRCA1; variants of uncertain significance; human genetic variation; protein function

IN an era of increasingly widespread genetic testing, DNA sequencing identifies many missense substitutions with unknown effects on protein function and disease risk. In the absence of genetic evidence, experimental measurement is the most reliable way to determine the functional impact of a variant of uncertain significance (VUS). However, initiating an experiment for each new variant observed in a gene is often impractical. When experiments are done, they are nearly always performed in a retrospective manner (Bouwman *et al.* 2013), such that the resulting data are not useful for the patient in whom the VUS was observed.

By prospectively measuring, in a high-throughput fashion, the consequences of all possible missense mutations on a gene's function, we can generate a look-up table for interpreting newly observed VUS. Although functional analysis at this scale is made possible by deep mutational scanning

(Fowler and Fields 2014), a central challenge is that any single assay may not recapitulate all the activities of a given protein in human disease. To address this challenge, we hypothesized that integrating the results of assays of multiple biochemical functions would strengthen estimates of the effects of mutations on disease risk (strategy outlined in Figure 1A). As a proof-of-concept, we initiated massively parallel functional analysis of BRCA1, a protein for which there are multiple biochemical functions as well as known pathogenic and benign missense substitutions to benchmark results.

BRCA1 has been subject to intense study since its implication in hereditary, early onset breast and ovarian cancer (Miki *et al.* 1994). All missense substitutions in BRCA1 that are known to be pathogenic occur in either the amino-terminal RING domain or the carboxy-terminal BRCT repeat (http://brca.iarc.fr/LOVD/home.php?select_db=BRCA1). Although the RING domain represents only 5% of the BRCA1 protein, 58% of the pathogenic missense substitutions occur within this domain. Sixty-two missense substitutions in the RING domain have been observed in patients, the general population, or tumor samples. Of these, only 22 have been classified—19 as pathogenic and 3 as benign (Supporting Information, Table S1)—by multifactorial models based on information from personal history, family history, and pathological profile and by A-GVGD (Tavtigian *et al.* 2006), a conservation-based, biological-effect prediction algorithm (reviewed in Lindor *et al.* 2012).
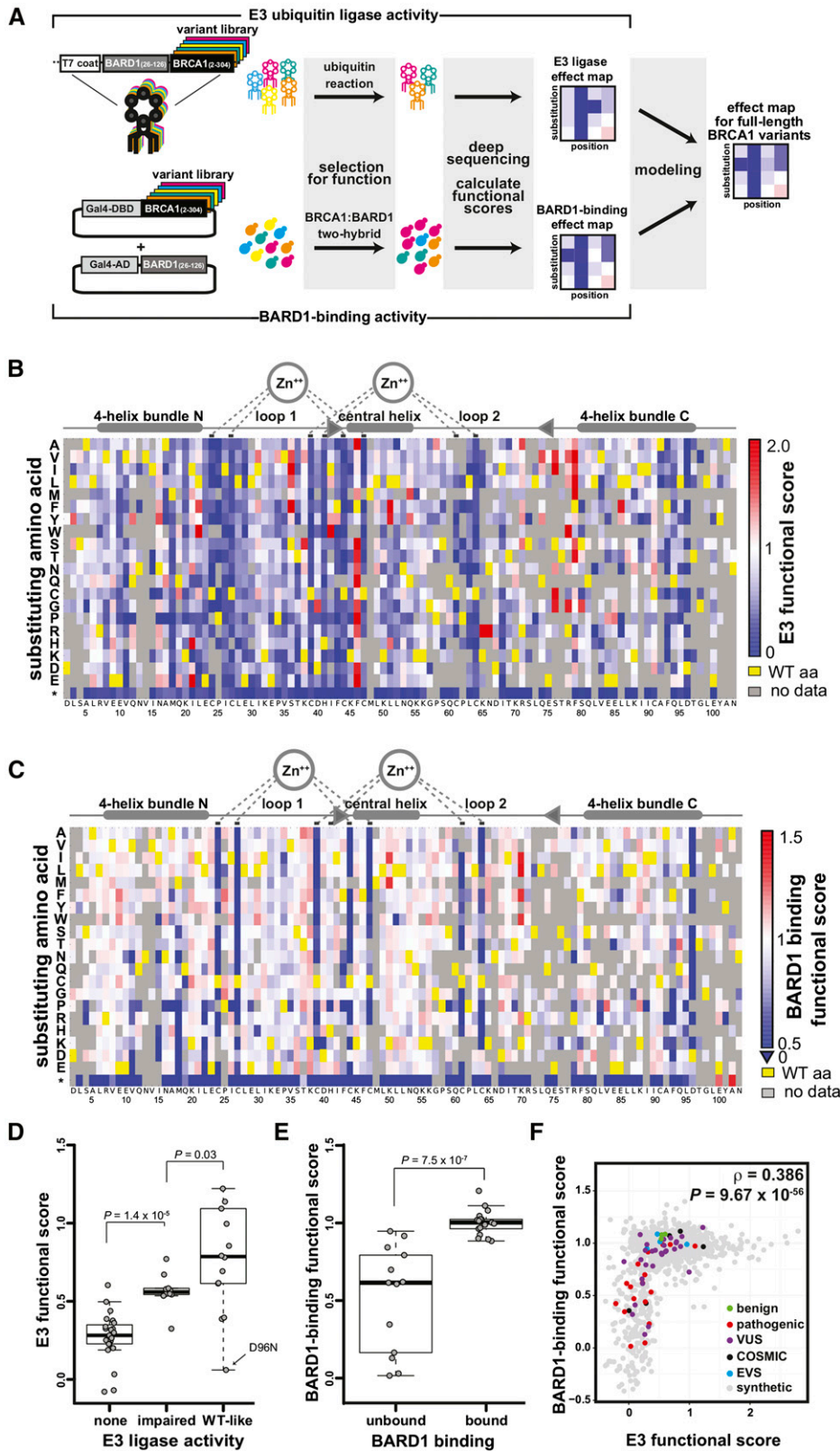
Figure 1 (A) Scheme for leveraging scores from parallelized assays for BRCA1 RING function into predictions for the function of the full-length BRCA1 protein in homology-directed DNA repair. (B-F) Scoring the E3 ligase and BARD1-binding activities of BRCA1 RING domain variants. (B) A sequence-function map of the effect of missense mutations in the BRCA1 RING domain on E3 ligase function. The functional score for each variant is the slope of the fit curve, normalized by setting stop codons to a score of 0 and the wild-type to a score of 1. Each position in BRCA1(2-103) is arranged along the x-axes, structural features of the RING domain are diagrammed above. The amino acid substitutions, grouped by side-chain properties, are on the y-axes. The E3 ligase scores range from improved activity versus wild-type (red), equivalent to wild-type (white), to less than wild-type (blue). Yellow represents the wild-type residue and gray missing or low confidence data. (C) A sequence-function map of the effect of missense mutations in the BRCA1 RING domain on BARD1-RING binding. Coloring as in panel B. (D) Comparison of the variant scores from the deep mutational scan for E3 ligase activity versus literature-reported E3 ligase activities for the same BRCA1 variants (Brzovic et al., 2003; Morris et al., 2006). The Wilcoxon rank sum test (WRST) was used to test for significant differences between the categories. The biggest outlier in the wild type-like category, D96N, not only performed poorly as an E3 ligase score but also failed to bind to BARD1 and to support homology-directed repair in cells (Table S2). (E) Comparison of BARD1-binding scores from the two-hybrid experiment versus literature-reported BARD1 binding by the same BRCA1 variants (Brzovic et al., 2003; Ransburgh et al., 2010). The WRST was used to test for significant differences between categories. (F) The relationship between the quality-filtered E3 ligase functional scores and the BARD1-binding scores. Colors indicate the clinical classification or database of origin for each variant.

Although BRCA1 has multiple roles in the cell, its activity in homology-directed DNA repair (HDR) is most closely associated with cancer risk (Moynahan et al. 1999; Towler et al. 2013). Cell-based HDR rescue assays on the full-length BRCA1 protein have been performed for a small number of variants (Ransburgh et al. 2010; Towler et al. 2013). However, those assays are too laborious to be applied to each possible BRCA1 variant. We therefore sought to implement

alternative BRCA1 functional assays that are more amenable to multiplexing.

The BRCA1 RING domain heterodimerizes with the RING domain of BARD1 to comprise an E3 ubiquitin ligase (Hashizume et al. 2001). The structural stability of the heterodimer is required for the stability of full-length BRCA1 (Wu et al. 2010). BRCA1 variants that cannot dimerize result in defects in HDR and loss-of-tumor suppression (Drost et al. 2011; Ransburgh et al. 2010). Assays for both BRCA1 E3 ligase activity and interaction with BARD1 are sensitive to amino acid substitutions that destabilize the structure of the heterodimer (Brzovic et al. 2003; Morris et al. 2006; Ransburgh et al. 2010). We therefore developed massively parallel assays (Fowler et al. 2010) to measure the impact of thousands of missense substitutions on these two functions.

To assay E3 ligase activity, we subjected an allelic series (Kitzman et al. 2015) (Figure S1) of the BRCA1 N terminus amino acids (2–304) to a phage display assay (Starita et al. 2013) that selects for protein variants capable of autoubiquitination (Christensen et al. 2007). We expressed BRCA1(2–304) variants on the surface of phage and selected for BRCA1 ubiquitination activity over five sequential rounds of selection in the presence of an E1, an E2, and Flag–ubiquitin by capturing phage with anti-Flag beads (Figure S2). Phages that encode active BRCA1 RING variants increase in abundance and those that encode inactive variants decrease in abundance over the multiple rounds of selection. We used deep sequencing to count each allele in the input phage population and after each round. We calculated E3 ligase scores by tracking the changes in the relative abundance of each allele during the selection (Araya et al. 2012). The scores were normalized such that the wild type had a score of one and the mean score for variants with premature termination codons had a score of zero. We obtained scores for 5154 of the 5757 possible single-amino-acid substitutions (Table S2). Using an input frequency threshold (Figure S3A), we filtered these to a high-confidence set corresponding to 3170 amino acid substitutions, with the six replicates having Spearman's rank correlation values between 0.76 and 0.83 (Figure S3B).

E3 ligase activity for variants with missense substitutions ranged from completely nonfunctional (scores of zero) to nearly three times higher than wild type. Scores for residues in the RING domain (2–103) are shown in Figure 1B and for residues 104–304 in Figure S4; all scores are reported in Table S2. As expected, substitutions in the residues that coordinate zinc ions and the residues in loop 1 and the central helix that contact the E2 enzyme (Brzovic et al. 2003) were the most intolerant to mutation (Figure 1B; Wilcoxon rank sum test (WRST), $P = 0.0008$), with the exception of Phe46, where most substitutions were hyperactivating. We compared the E3 ligase scores to previous work by splitting the published activities of BRCA1 RING domain variants in in vitro ubiquitination assays (Brzovic et al. 2003; Morris et al. 2006) into three categories: completely nonfunctional, impaired, or wild-type like. E3 ligase scores corresponding to variants in the nonfunctional category were lower than

those in the impaired category (WRST, $P = 1.4 \times 10^{-5}$), which were in turn lower than those in the wild-type-like category (WRST, $P = 0.03$, Figure 1D).

In separate experiments, we used a multiplexed yeast two-hybrid assay to select for the ability of BRCA1 RING domain (2–103) (Brzovic et al. 2001) variants to interact with the RING domain of BARD1. The DNA-binding domain of the yeast transcription factor Gal4 was fused to the BRCA1(2–304) allelic series and the Gal4 activation domain was fused to BARD1(26–126) (Figure S5). Here, BRCA1 binding to BARD1 drives the expression of a selectable reporter gene such that yeast expressing BRCA1 variants that bind to BARD1 increase in abundance during the selection and those expressing nonfunctional variants decrease. We used deep sequencing to quantify the relative abundance of alleles after transformation into the yeast and at multiple time points during the selection (Materials and Methods and Table S2). We calculated a BARD1-binding score for 1855 of 1938 possible amino acid substitutions, excluding the carboxy-terminal 201 amino acids, which were required only for the autoubiquitination assay but not the BARD1-binding assay (Brzovic et al. 2001). Using an input frequency threshold, we filtered these to a high-confidence subset corresponding to 1529 substitutions, whose scores were highly reproducible ($\rho = 0.82$–0.95, Figure S6 and Table S2).

Overall, BARD1-binding scores agreed with what is known about the RING–RING interaction. The residues that coordinate the zinc ions were the most intolerant to substitution with the exception of H41 (Brzovic et al. 2001) (Figure 1C). The effect size for most other substitutions was small, which was expected given the large interface between the two RING domains (Brzovic et al. 2001). We compared our results with those published for co-immunoprecipitation of BRCA1 RING domain variants with BARD1 (Brzovic et al. 2003; Ransburgh et al. 2010). While the scores from the yeast two-hybrid BARD1-binding assay were lower for BRCA1 variants reported not to bind to BARD1 (WRST, $P = 7.5 \times 10^{-7}$), these scores spanned the entire range from zero to one (Figure 1E). Intermediate BARD1-binding scores for BRCA1 variants with weak or no BARD1 binding in co-immunoprecipitation assays may derive from differences in variant thermostability between the yeast assay (carried out at 30°) and the mammalian cell culture assay (carried out at 37°), and the in vivo transcriptional readout of the two-hybrid assay being more sensitive than co-immunoprecipitation.

We compared the E3 ligase scores to the BARD1-binding scores and observed that neither assay was sufficient alone to accurately discriminate BRCA1 variants with respect to their pathogenicity (Figure 1F, colored points). Because BARD1-binding is required for E3 ligase function, the scores from both assays were modestly correlated ($\rho = 0.386$; $P = 9.67 \times 10^{-56}$), but many more positions were intolerant to substitutions in the E3 ligase assay (Figure 1F). Although the E3 ligase activity of BRCA1 may not be required for HDR and therefore tumor suppression (Reid et al. 2008; Shakya et al. 2011), the E3 ligase and BARD1-binding activities likely reflect the structural

stability of the RING domain. Indeed both assays had some power to discriminate BRCA1 variants with respect to their pathogenicity (Figure 1F, colored points). We hypothesized that these two rich mutational data sets could be combined to accurately identify deleterious substitutions in the BRCA1 RING domain.

A test of whether the results from these high-throughput biochemical assays can be used to discriminate disease risk alleles needs "gold standards" as benchmarks. Since only 22 mutations in the BRCA1 RING domain have been classified for pathogenicity, we required a larger set of BRCA1 variants with established, disease-relevant functional consequences. Therefore, we tested additional full-length BRCA1 variants in the assay that best correlates with tumor suppression: rescue of HDR at an induced double-strand break by expression of a BRCA1 variant following siRNA knockdown of endogenous BRCA1 (Figure 2A). We curated results from this assay (Ransburgh *et al.* 2010; Towler *et al.* 2013) for 17 missense substitutions in the BRCA1 RING domain and tested an additional 28 (Figure 2B) for a total of 45. Of the 19 known pathogenic mutants, 8 have now been tested for HDR rescue. As expected, after excluding R71G, a variant that affects BRCA1 splicing (Vega *et al.* 2001), these pathogenic mutants all had low HDR rescue scores (mean = 0.19, max = 0.33) that separate them from the three known benign variants, which have much higher scores (mean = 0.88, min = 0.77; Figure 2B and Table S2). We defined a BRCA1 HDR rescue score of 0.53—the value midway between the average HDR rescue score for known pathogenic BRCA1 variants and the average score for known benign variants—as the inflection point for discriminating between functional and nonfunctional variants, as was done for BRCA2 (Guidugli *et al.* 2014). With this inflection point, the HDR rescue assay has 100% sensitivity and 100% specificity.

We then asked whether models trained on the E3 ligase and BARD1-binding scores can predict the effects on HDR rescue of substitutions in the full-length protein. We evaluated the accuracy of several models using leave-one-out cross-validation (LOOCV), wherein we serially predicted HDR rescue scores for each of the 44 missense substitutions for which we had empirical HDR rescue and functional scores from models fit on the 43 remaining variants. We first compared the performance of models tested on scores from the E3 ligase and BARD1-binding assays alone or in combination. A linear model based on scores from both assays outperformed linear models based on scores from either assay alone (Figure 3, A and B). However, because we observed a nonlinear relationship between E3 ligase and BARD1-binding scores (Figure 1F), we tested whether nonlinear models would improve HDR prediction results. A support vector regression (SVR) model trained on E3 ligase scores and BARD1-binding scores yielded the best predictive power for HDR rescue (Figure 3C).

We next replaced our experimental data with computational predictions from several popular variant effect prediction algorithms (Grantham 1974; Ng and Henikoff 2003; Cooper *et al.* 2005; Tavtigian *et al.* 2006; Adzhubei *et al.*

2010; Kircher *et al.* 2014), which incorporate evolutionary constraints and/or chemical differences between amino acid side chains, and repeated the model training procedure. Individually, these prediction-based models performed poorly at predicting a substitution's effect on HDR (Figure 3D, white bars, and Figure S7). Although A-GVGD was the best performing algorithm, it yielded higher error and lower correlation than all experimentally-based models (Figure 4D and Figure S7F). Furthermore, when we added the A-GVGD predictions to the experimental data and trained a hybrid model, performance was not enhanced over the experimentally based models (Figure 3D, gray bar, and Figure S7G). A plausible explanation for the comparatively poor performance of models trained on computational predictions is that they are largely based on features that are not specific to BRCA1 (*e.g.*, Grantham chemical difference scores) or on evolutionary constraint information that captures organismal fitness over evolutionary timescales, which may poorly discriminate subtle and strong molecular effects on BRCA1 function.

Because the SVR model based on combined functional data sets from the two assays was the most accurate, we used it to predict HDR scores for the 1287 BRCA1 RING domain missense variants with both high-confidence E3 ligase and BARD1-binding scores (Figure 4, A–C and Table S2), 1225 of which have not yet been reported in clinical sequencing. The distribution of predicted HDR scores is bimodal; 785 missense substitutions are predicted to have little effect on HDR, with predicted rescue scores >0.77 (Figure 4A). Conversely, 160 substitutions are predicted to be damaging to HDR, with scores <0.33; these variants would potentially increase the risk of hereditary breast and ovarian cancer. Based on this SVR modeling, only 342 variants have predicted scores in the indeterminate region between functional and nonfunctional.

As expected, predicted HDR scores for most of the 19 known pathogenic mutants in the BRCA1 RING domain are low (Figure 4B). Excluding pathogenic mutants known to affect splicing or used to train the model leaves 10 pathogenic mutants. All 10 have predicted HDR scores <0.53, the threshold for classifying a variant as functional. Nine have predicted HDR scores <0.33, the maximum empirical HDR rescue score for a known pathogenic mutant. Thus, our model demonstrates strong performance in predicting HDR activity of known variants (Figure 4B and Table S2). For 31 VUS identified in patients, predicted HDR scores range from near zero to wild-type-like, with 8 of 31 <0.53 and 5 <0.33, suggesting that a substantial fraction of individuals with VUS diagnoses may carry pathogenic BRCA1 alleles.

The data in Figure 4C represent a prospective map or look-up table for the effects of missense substitutions in the RING domain of BRCA1 on HDR function. This experimentally-derived map is more accurate than any map that could be generated using current computational tools. In terms of defining BRCA1 activity, these systematic mutational analyses uncovered positions in the four-helix bundle that show extreme sensitivity to substitution. For example, V11 does not tolerate
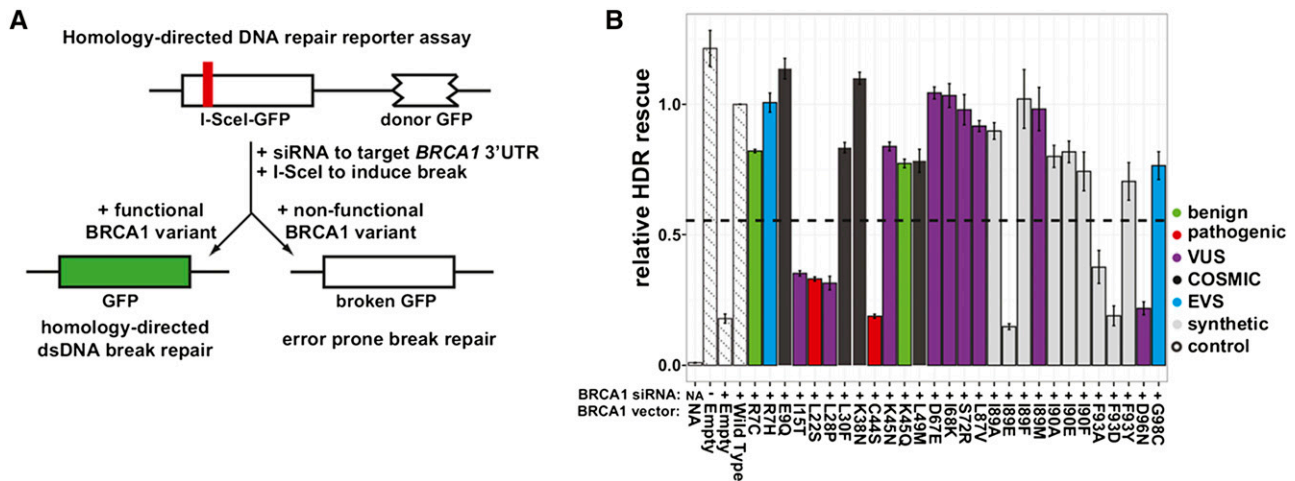
Figure 2 Testing BRCA1 variants for their ability to rescue homology-directed DNA repair. (A) Integrated into the genome of the HDR reporter strain is one copy of the GFP gene containing an I-SceI homing endonuclease site that introduces an in-frame stop codon, along with another copy of the GFP gene lacking both its start and stop codons that functions as a donor for DNA repair (Pierce *et al.* 2001). The cell line is depleted for BRCA1 by transfection with an siRNA that targets the 3′-UTR of the endogenous gene. I-SceI and a full-length variant of BRCA1 are then transfected into the cells. After 3 days, the GFP+ population is assessed by flow cytometry. (B) The wild-type normalized percentage of cells that were GFP+ in the BRCA1 HDR rescue assay is shown. Experiments were performed in triplicate and error bars represent the standard error. siRNA, BRCA1 variant, and clinical classification or database of origin is indicated by color. Dashed horizontal line represents the midpoint between the average HDR scores for known pathogenic and benign variants.

substitutions with charged or amine-containing polar amino acids; M18 does not tolerate charged, polar, or aromatic substitutions; and F93 and D96 do not tolerate any substitutions. Our data support the idea some variants with defects in the E3 ligase activity are not compromised for HDR and tumor suppression (Reid *et al.* 2008; Shakya *et al.* 2011). The benign variants R7C and D67Y showed no binding defect with BARD1 and were able to rescue HDR but they performed poorly in the E3 ligase selections. However, they may retain enough E3 ligase activity to satisfy a possibly low threshold of requisite activity.

Our results demonstrate the power of empirical measurements to assess the impact of missense variants on complex protein functions. Thus, we envision that massively parallel experiments to measure the effects of large numbers of substitutions will meet an urgent need in the clinical translation of genetic information.

Materials and Methods

BRCA1(2-304) single codon substitution library construction by the Programmed Allelic Series method

Oligonucleotides, 90-mers, to direct the single codon mutagenesis of BRCA1 were synthesized on and released from a 12,000-feature array by Custom Array (Bothell, WA) (example in Table S3, BRCA1_00284.0). The BARD1(26–126)–GS–BRCA1(2–304) fusion open reading frame (ORF) (Christensen *et al.* 2007) was moved to the pGEM vector and the *Eco*RI site in BRCA1 was destroyed. This fragment of BRCA1 was used as a template for PALS mutagenesis (Kitzman *et al.* 2015). Sixteen base random barcodes (16N) were added 3′ of the stop codon in the final PCR step. The ligation of the

final mutagenized and barcoded amplicon was transformed into DH10B electromax cells (NEB) and yielded 250,000 unique transformants of the pGEM_BARD1_GS_BRCA1-var_barcode library.

Subassembly to match 16N barcodes to BRCA1 variants

Since BRCA1(2–304) is too long to be sequenced in one pass by current Illumina technology, we developed a method to create randomly shortened contigs that could be grouped by barcode to use in an assembly method call tag-directed read grouping or subassembly (Hiatt *et al.* 2010). A total of 5 μg of the plasmid pGEM_BARD1_GS_BRCA1-var was cut at the 5′ end of the BRCA1 ORF with *Bam*HI and purified. The purified DNA was digested using the double-strand exonuclease Bal-31 (NEB), 1 unit Bal31 per 1.6 pmol DNA ends at 30°. Aliquots were taken at 0, 3, 7, 11, 13, and 15 min and placed in the DNA-binding buffer from the Zymo clean and concentrate kit to stop the reactions. One-fifth of the digested and cleaned DNA was cut with *Hin*dIII and examined by PAGE to determine the degree of digestion. DNA from all time points was pooled and treated with End-it (Epicentre) to blunt and phosphorylate the ends. Blunt-ended, cleaned DNA was A-tailed using goTaq (NEB) and cleaned again. A double-stranded linker containing the Tru-seq Illumina Read 2 primer was ligated onto the A-tailed DNA (W-E4B-subassembly-linker and phosphorylated C-E4B-subassembly linker). The linkered and cleaned DNA was cut with *Sac*I (NEB) to separate the ORF and barcode from the rest of the plasmid. Primers that annealed to the linker and plasmid DNA directly 3′ of the barcode that contain the p5 and p7 Illumina cluster generating sequences (newBRCA1-side_R_CG1 and BRCA1-side_R_CG2) were used to amplify the fragments and barcode for Illumina sequencing in reactions containing the high-fidelity polymerase KAPA HFHSRM and SYBR green
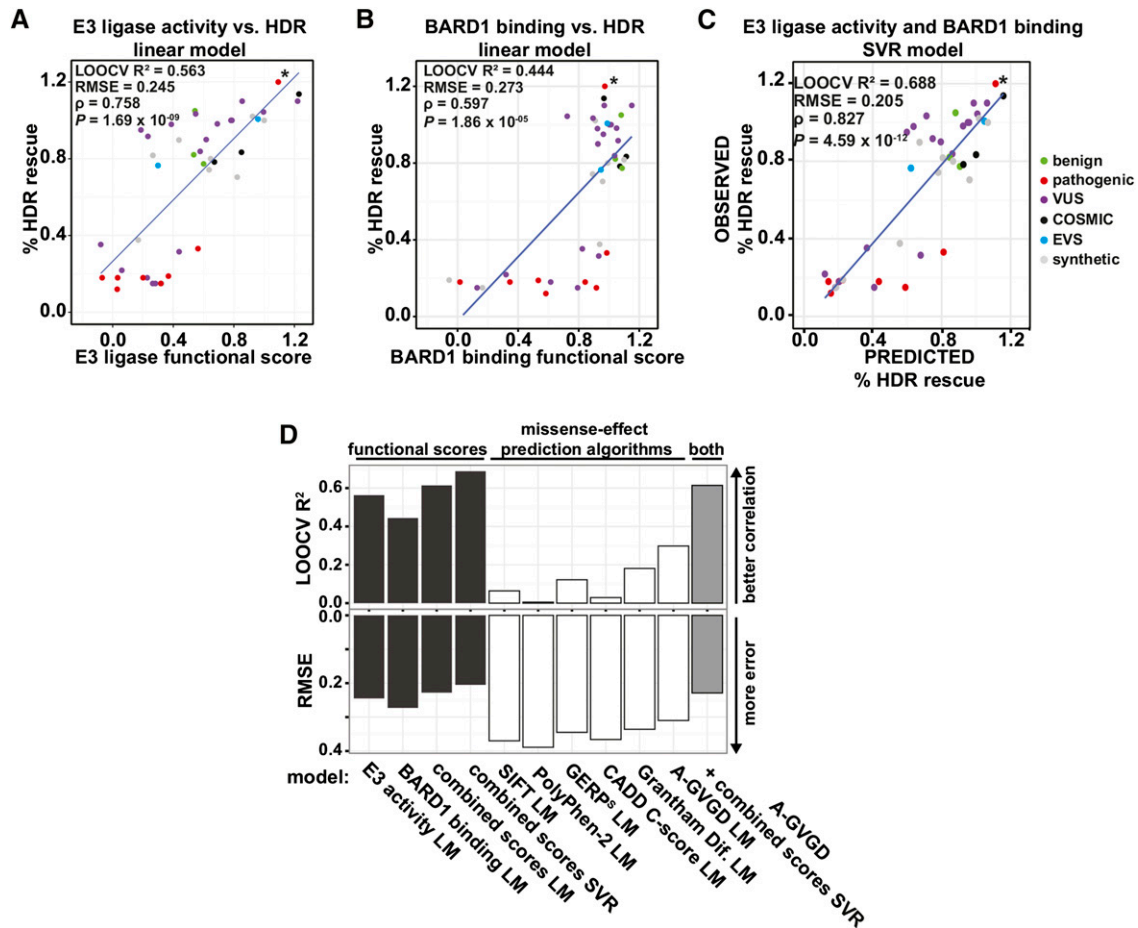
Figure 3 Scores from massively parallel E3 ligase and BARD1-binding assays on BRCA1 RING domain variants are better predictors of the HDR activity of the full-length protein. The linear relationship of the E3 ligase scores (A), BARD1-binding scores (B), and HDR scores. (C) A support vector regression (SVR) model of HDR rescue scores from the combination of the E3 ligase and BARD1 binding functional scores. Variants are colored by database of origin. The blue line represents the least-squares fit of the displayed data. Known pathogenic splice variant R71G is marked with an asterisk. (D) Experimentally or computationally derived values for the effect of missense variants on protein function were used to predict the effect on HDR. The LOOCV R^2 and RMSE for each model is indicated. The RMSE of LOOCV indicates the average distance between the HDR rescue predictions and the true HDR rescue scores, and the LOOCV R^2 is the overall correlation between predicted and observed values; low RMSE and high R^2 indicate better predictive power. For A-GVGD, the Grantham deviation value was used. Source of HDR predictions is indicated by color, linear model (LM), and SVR.

[conditions: 95° 3:00 (98° 0:20, 63° 0:15, 72° 1:50) × 12–15]. The amplicons were sequenced on an Illumina HiSeq2000 in paired-end, 2 × 101 run mode and with an Illumina MiSeq paired-end, 2 × 250 kit.

Reads were filtered for quality and grouped by the sequence of the 16-base barcode. A Smith–Waterman algorithm was used to align the grouped reads to the wild-type BRCA1(2–304) sequence and a consensus sequence was determined for each barcode group as in Hiatt *et al.* (2010) and Patwardhan *et al.* (2012). A minimum quality score of 20 was required for a base to contribute to an assembly. Full-length BRCA1(2–304) sequences were filtered for quality by requiring that a given base in the assembly was observed at least twice and was present at an intra-tag group allele frequency of one for positions covered by two to four reads or a frequency of at least 0.8 for positions covered by five or more reads. If these conditions were not met the assembly was discarded. We assembled 128,237 barcoded variants, of which 60,256

corresponded to 5156 single-amino-acid changes out of the possible 5757 (89% of the 19 substitutions × 303 codons) in BRCA1(2–304) (see Figure S1). A database of barcodes and their associated full-length BRCA1(2–304) assembly was created to facilitate linking barcodes sequenced from the experimental samples to the full-length subassemblies.

Phage-based E3 ligase assays

The BARD1(26–126)_glycine–serine linker_BRCA1(2–304) library was subcloned from pGEM_BARD1_GS_BRCA1-var_barcode by cutting and gel purifying the *Eco*RI and *Hin*dIII fragment and ligating into the genome of T7–Select 10-3b bacteriophage. Phage genomic DNA was packaged into phage particles, the number of ligation/packaging events was estimated by titer as 2.56 × 10^7 plaque-forming units (PFU), and the phages were amplified in *E. coli* strain BLT5403 according to the T7Select Cloning Kit instructions (EMD Millipore). The selections for functional BRCA1(2–304) phages were performed as in
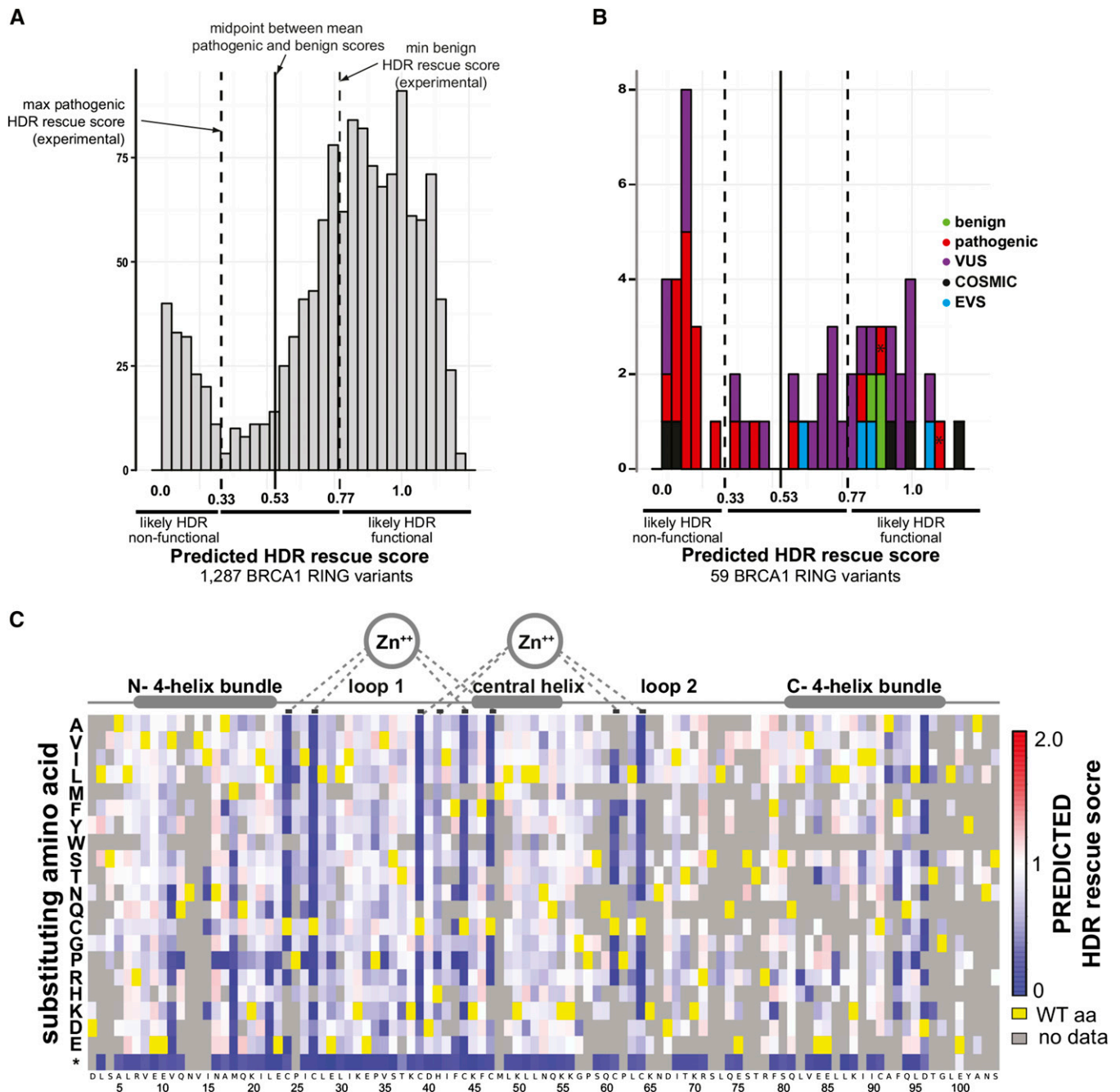
Figure 4 Predicted HDR rescue scores for 1287 BRCA1 RING variants create a prospective map of the effect of missense substitutions. (A) A histogram of the predicted HDR scores for the 1287 BRCA1 RING variants with both high-confidence E3 ligase and BARD1-binding scores. (B) A histogram of the 59 of the 62 BRCA1 RING variants found in the human population, clinical classification, or database of origin is indicated by color. Known splice variants R71G and R71K are marked with an asterisk. (C) Sequence-function map of the predicted HDR rescue scores for BRCA1 RING variants. Colors are centered on 1.0 as wild type (white). Structural features of the BRCA1 RING domain are diagrammed above.

Starita *et al.* (2013) with these differences: amplified phage were never stored more than 24 hr before a sequential round of selection and the 50-μl ubiquitination reactions contained 20 μl ($\sim$1 × 10^7 PFU) of amplified phage, 2 mM ATP, 5 mM MgCl2, 1 μM wheat E1 ubiquitin activating enzyme, 4 μM UBE2D3 (UbcH5c), and 8 μM Flag-tagged ubiquitin.

DNA from the initial amplified phage population and amplified phage from each replicate from each of five rounds

of selection was purified from 200 μl of lysate by phenol chloroform extraction. Barcodes were PCR amplified in two sequential reactions. The first reaction contained primers jkA0390_BBcplxcheckF and E4B-index01-8_CG-R or T7_barcodes_common primer_R and 200 ng of phage DNA in reactions containing the high-fidelity polymerase Phusion (NEB), 2 mM added MgCl2, and SYBR green [conditions: 95° 3:00 (98° 0:20, 63° 0:15, 72° 1:50) × 10–13]. Reaction

products were monitored by qPCR and removed during exponential amplification. The first reactions were purified using the Zymo clean and concentrate kit. One-tenth of that product was amplified with JK19 and one of the index containing primers E4B-index01-8_CG-R or common_index_primers such as NexV2ad2_A1 [conditions: 95° 3:00 (98° 0:20, 63° 0:15, 72° 1:50) × 4–6]. Again, reaction products were monitored by qPCR and removed during exponential amplification. Reaction products were treated with exonuclease I (Affymetrix) for 15 min at 37° then purified using the Zymo clean and concentrate kit. Samples were multiplexed and sequenced using primer jkA0390_BBcplxcheckF on an Illumina GAIIx or HiSeq2000 in single end mode.

Yeast two-hybrid-based deep mutational scan for BRCA1-BARD1 binding

The Gal4 DNA-binding domain (Gal4DBD) was amplified from pOBD2 (Cagney *et al.* 2000) using primers *Spe*I_Gal4DBD_F and *Spe*I_Gal4DBD_R and cloned into p414–ADH (Mumberg *et al.* 1995). The BRCA1(2–304) variant library was excised from pGEM_BARD1_GS_BRCA1-var_barcode library by digestion with *Bam*HI (NEB) and *Pst*I (NEB) and ligated into p414_Gal4DBD to create p414_Gal4DBD_BRCA1_var_barcode, yielding $\sim 1.16 \times 10^5$ total transformants. BARD1(26–126) was amplified from pGEM_BARD1_GS_BRCA1 using primers *Eco*RI_BARD1_Ln_F and *Nco*I_BARD1_Stop_R and cloned into pOAD (Cagney *et al.* 2000) containing the Gal4 transcriptional activation domain.

The *S. cerevisiae* strain, PJ69a (James *et al.* 1996), containing pOAD_BARD1 was transformed (Melamed *et al.* 2013) with the p414_Gal4DBD_BRCA1_var_barcode library with a yield of $\sim 1.26 \times 10^6$ total transformants. Transformed yeast were transferred to 40 ml SD–Leu–Trp, cultured overnight and stored in 6.7 optical density units (ODU) aliquots at −80°.

Two independent experiments (A and B) were performed, each consisting of three independent selections: 12.5 ODU (A) or four ODU (B) of cells were collected from each culture at each time point for sequencing. Each experiment began by culturing one frozen aliquot of PJ69a transformed with pOAD_BARD1 and p414_Gal4DBD_BRCA1_var_barcode in SD–Leu–Trp to logarithmic phase (A, 1.01 OD/ml; B, 0.83 OD/ml). Cells from this input population were collected for sequencing and for back dilution into the selection medium (SD–His–Leu–Trp + 10 mM 3-amino-1,2,4 triazole (Sigma), A, 5 OD to 200 ml; B, 2 OD to 100 ml) in triplicate. Each replicate was cultured to logarithmic phase (A, 18 hr, 1.1 OD/ml; B, 16 hr, 0.7 OD/ml) after which cells were collected for sequencing and back diluted into fresh selection medium (A, 1 OD to 100 ml; B, 0.6 OD to 100 ml). Each replicate was again cultured to logarithmic phase (A, 37 hr, 0.62 OD/ml; B, 40.5 hr, 0.67 OD/ml), after which cells were collected for sequencing and back diluted into fresh selection medium (A, 12.5 OD to 125 ml; B, 1.1 OD to 100 ml). Each replicate was again cultured to logarithmic phase (A, 45 hr, 0.43 OD/ml; B, 64 hr, 1.4 OD/ml) and the final time point was collected.

Plasmid DNA was isolated from the input and samples collected during the selection for growth in the -histidine media using a Zymoprep Yeast Plasmid Miniprep II kit (Zymo Research). Sequencing amplicons were prepared individually for each sample by two successive PCR reactions using Phusion high-fidelity DNA polymerase. In the first reaction, primers jkA0390_BBcplxcheckF and BRCA1-Y2H_commonLinker_R were used to amplify the barcoded region of half of the prepared p414_Gal4DBD_BRCA1_var_barcode plasmid. Of the first reaction, 4% was amplified with primers JK19 and NexV2ad2_XX to append Illumina cluster generating sequences and a unique sample index sequence. Reaction products of all PCR reactions were monitored on a mini-opticon qPCR machine (Bio-Rad) and removed during exponential amplification. Samples were purified, multiplexed, and sequenced using primer jkA0390_BBcplxcheckF on a HiSeq2000 in single-end mode.

Slope calculations and normalization

The Illumina reads that matched to barcodes associated with full-length assemblies were retained and unmatched barcodes were discarded. The matched barcodes were converted to the sequence of the full length BRCA1(2–304) assembly and the Enrich software package (Fowler *et al.* 2011) was used to determine locations and identity of substitutions and to tally the number of times each variant appeared in each population (Table S2).

Sequencing read counts corresponding to a given variant were equal to the sum of read counts from all barcodes matching that variant. For each time point, frequencies were calculated for all variants as the variant's read count divided by the sum of all read counts at that time point. Variants that dropped out (cannot be found in the selected populations) had their frequencies set to the lowest possible frequency at that time point. Ratios were calculated as the variant's frequency in the selected time point divided by its frequency in the input library. For each variant, a linear model was fit by least squares to the log ratios over time using numpy.polyfit. The inverse log of this slope corresponds to the percentage change in frequency per unit time. To obtain a normalized score, the average inverse log of the slope for all stop codons was subtracted from all inverse-log-slopes so that stop codons, on average, have a score of 0. These 0 centered values were then divided by the wild-type (WT) inverse-log-slope so that a score of 1 corresponds to WT function.

The normalized score for variant *i* is

$$\frac{2^{\text{Slope}_i} - \sum_0^m 2^{\text{Slope}_m}}{2^{\text{Slope}_{\text{WT}}}},$$

where *m* is the number of stop codons from positions 2–103 and all slopes were fit to the log ratios at each time point. A conservative estimate of the standard deviation of the slopes was generated using a Loess curve to model the relationship between frequency in the input population and variance across all replicates (based on the assumption that the variance is

related to the frequency in the input population; see Figure S3 and Figure S6). For each variant, the conservative variance was set to whichever was larger: the variance across all replicates or the value of the Loess curve evaluated at the number of input reads for that variant. This estimate was used to generate the reported confidence intervals (Table S2). Additionally, we used cutoff based on the number of input reads to determine the high-confidence data set that would be used for the final HDR predictions. The heuristic to determine the cutoff is described in Figure S3 and Figure S6. HDR predictions were made only for variants with high-confidence scores in both the E3 ligase and BARD1-binding assays. Finally, a permutation test was used to compare each variant's slopes to the WT slopes across all replicates. The average difference between paired slopes was used as the test statistic and 10,000 permutations were performed for each variant (Table S2).

Full-length BRCA1 variant construction and HDR assays

Mutations in the BRCA1 RING domain were made by overlap-extension PCR and subcloned into the HindIII and EcoRI sites of pcDNA3–HA–BRCA1 (plasmid described in Chiba and Parvin 2001). All constructs were verified by Sanger sequencing. BRCA1 rescue of HDR assays were performed in triplicate as in Ransburgh et al. (2010). All BRCA1 HDR rescue scores are normalized to that of the wild-type protein at HDR rescue = 1. The maximum HDR score for known pathogenic variant of BRCA1 is 0.33. Seven pathogenic variants (excluding splice variant R71G) have been tested for HDR rescue with a mean score of 0.19. Of the only three known benign BRCA1 RING domain variants, all have been tested for HDR rescue and have a minimum score of 0.77 with an average score 0.88. We defined a BRCA1 HDR rescue score of 0.53—the value midway between the average HDR rescue scores for known pathogenic BRCA1 variants and the average scores for known benign variants—as the inflection point for discriminating between functional and nonfunctional variants, as was done for BRCA2 (Guidugli et al. 2014).

HDR prediction model building and testing

We obtained SIFT, Polyphen-2, GERP++, and CADD values from the CADD database (Kircher et al. 2014) and references therein (http://cadd.gs.washington.edu/download). For every possible amino acid substitution in BRCA1 (2-103), we obtained Grantham chemical difference values from Grantham(1974), and GVGD values from the A-GVGD BRCA1 web-tool (http://agvgd.iarc.fr/agvgd_input.php). Grantham deviation (GD) values were used to predict HDR rescue scores.

All models were fit and cross-validated using the R package caret (Kuhn 2008). Linear models were fit by least squares. Support vector regression models used the radial basis function kernel and were validated using a nested cross validation scheme (Cawley and Talbot 2010). Briefly, for each step of the LOOCV, an inner LOOCV loop was used to determine model performance on each C and sigma pair in the tested parameter space and the best performing model (based on root mean square error, RMSE) was used to predict the holdout in the outer loop. The range of sigma values tested in the inner loop was determined using the sigest function from the R package kernlab and the C values tested were 0.1, 1, 2, 5, 10, 100, and 1000. The final model used for HDR predictions was chosen by picking the parameter pair with the lowest average RMSE across all iterations of the outer loop (Y2H and E3 model—$C = 5$ and sigma = 0.1633448, Y2H, E3; GVGD model—$C = 5$ and sigma = 0.08220825).

Literature Cited

Adzhubei, I. A., S. Schmidt, L. Peshkin, V. E. Ramensky, A. Gerasimova et al., 2010 A method and server for predicting damaging missense mutations. Nat. Methods 7: 248–249.

Araya, C. L., D. M. Fowler, W. Chen, I. Muniez, J. W. Kelly et al., 2012 A fundamental protein property, thermodynamic stability, revealed solely from large-scale measurements of protein function. Proc. Natl. Acad. Sci. USA 109: 16858–16863.

Bouwman, P., H. van der Gulden, I. van der Heijden, R. Drost, C. N. Klijn et al., 2013 A high-throughput functional complementation assay for classification of BRCA1 missense variants. Cancer Discov. 3: 1142–1155.

Brzovic, P. S., P. Rajagopal, D. W. Hoyt, M. C. King, and R. E. Klevit, 2001 Structure of a BRCA1–BARD1 heterodimeric RING-RING complex. Nat. Struct. Biol. 8: 833–837.

Brzovic, P. S., J. R. Keeffe, H. Nishikawa, K. Miyamoto, D. Fox et al., 2003 Binding and recognition in the assembly of an active BRCA1/BARD1 ubiquitin-ligase complex. Proc. Natl. Acad. Sci. USA 100: 5646–5651.

Cagney, G., P. Uetz, and S. Fields, 2000 High-throughput screening for protein–protein interactions using two-hybrid assay. Methods Enzymol. 328: 3–14.

Cawley, G. C., and N. L. C. Talbot, 2010 On over-fitting in model selection and subsequent selection bias in performance evaluation. J. Mach. Learn. Res. 11: 2079–2107.

Chiba, N., and J. D. Parvin, 2001   Redistribution of BRCA1 among four different protein complexes following replication blockage. J. Biol. Chem. 276: 38549–38554.

Christensen, D. E., P. S. Brzovic, and R. E. Klevit, 2007   E2-BRCA1 RING interactions dictate synthesis of mono- or specific polyubiquitin chain linkages. Nat. Struct. Mol. Biol. 14: 941–948.

Cooper, G. M., E. A. Stone, G. Asimenos, N. I. S. C. C. S. Program, E. D. Green et al., 2005   Distribution and intensity of constraint in mammalian genomic sequence. Genome Res. 15: 901–913.

Drost, R., P. Bouwman, S. Rottenberg, U. Boon, E. Schut et al., 2011   BRCA1 RING function is essential for tumor suppression but dispensable for therapy resistance. Cancer Cell 20: 797–809.

Fowler, D. M., and S. Fields, 2014   Deep mutational scanning: a new style of protein science. Nat. Methods 11: 801–807.

Fowler, D. M., C. L. Araya, S. J. Fleishman, E. H. Kellogg, J. J. Stephany et al., 2010   High-resolution mapping of protein sequence-function relationships. Nat. Methods 7: 741–746.

Fowler, D. M., C. L. Araya, W. Gerard, and S. Fields, 2011   Enrich: software for analysis of protein function by enrichment and depletion of variants. Bioinformatics 27: 3430–3431.

Grantham, R., 1974   Amino acid difference formula to help explain protein evolution. Science 185: 862–864.

Guidugli, L., A. Carreira, S. M. Caputo, A. Ehlen, A. Galli et al., 2014   Functional assays for analysis of variants of uncertain significance in BRCA2. Hum. Mutat. 35: 151–164.

Hashizume, R., M. Fukuda, I. Maeda, H. Nishikawa, D. Oyake et al., 2001   The RING heterodimer BRCA1–BARD1 is a ubiquitin ligase inactivated by a breast cancer-derived mutation. J. Biol. Chem. 276: 14537–14540.

Hiatt, J. B., R. P. Patwardhan, E. H. Turner, C. Lee, and J. Shendure, 2010   Parallel, tag-directed assembly of locally derived short sequence reads. Nat. Methods 7: 119–122.

James, P., J. Halladay, and E. A. Craig, 1996   Genomic libraries and a host strain designed for highly efficient two-hybrid selection in yeast. Genetics 144: 1425–1436.

Kircher, M., D. M. Witten, P. Jain, B. J. O'Roak, G. M. Cooper et al., 2014   A general framework for estimating the relative pathogenicity of human genetic variants. Nat. Genet. 46: 310–315.

Kitzman, J. O., L. M. Starita, R. S. Lo, S. Fields, and J. Shendure, 2015   Massively parallel single amino acid mutagenesis. Nat. Methods.

Kuhn, M., 2008   Building predictive models in R using the caret package. J. Stat. Softw. 28(5).

Lindor, N. M., L. Guidugli, X. Wang, M. P. Vallée, A. N. A. Monteiro et al., 2012   A review of a multifactorial probability-based model for classification of BRCA1 and BRCA2 variants of uncertain significance (VUS). Hum. Mutat. 33: 8–21.

Melamed, D., D. L. Young, C. E. Gamble, C. R. Miller, and S. Fields, 2013   Deep mutational scanning of an RRM domain of the Saccharomyces cerevisiae poly(A)-binding protein. RNA 19: 1537–1551.

Miki, Y., J. Swensen, D. Shattuck-Eidens, P. A. Futreal, K. Harshman et al., 1994   A strong candidate for the breast and ovarian cancer susceptibility gene BRCA1. Science 266: 66–71.

Morris, J. R., L. Pangon, C. Boutell, T. Katagiri, N. H. Keep et al., 2006   Genetic analysis of BRCA1 ubiquitin ligase activity and its relationship to breast cancer susceptibility. Hum. Mol. Genet. 15: 599–606.

Moynahan, M. E., J. W. Chiu, B. H. Koller, and M. Jasin, 1999   Brca1 controls homology-directed DNA repair. Mol. Cell 4: 511–518.

Mumberg, D., R. Müller, and M. Funk, 1995   Yeast vectors for the controlled expression of heterologous proteins in different genetic backgrounds. Gene 156: 119–122.

Ng, P. C., and S. Henikoff, 2003   SIFT: predicting amino acid changes that affect protein function. Nucleic Acids Res. 31: 3812–3814.

Patwardhan, R. P., J. B. Hiatt, D. M. Witten, M. J. Kim, R. P. Smith et al., 2012   Massively parallel functional dissection of mammalian enhancers in vivo. Nat. Biotechnol. 30: 265–270.

Pierce, A.J., P. Hu, M. Han, N. Ellis, and M. Jasin, 2001   Ku DNA end-binding protein modulates homologous repair of double-strand breaks in mammalian cells. Genes Dev. 15: 3237–3242.

Ransburgh, D. J. R., N. Chiba, C. Ishioka, A. E. Toland, and J. D. Parvin, 2010   Identification of breast tumor mutations in BRCA1 that abolish its function in homologous DNA recombination. Cancer Res. 70: 988–995.

Reid, L. J., R. Shakya, A. P. Modi, L. Lokshin, J.-T. Cheng et al., 2008   E3 ligase activity of BRCA1 is not essential for mammalian cell viability or homology-directed repair of double-strand DNA breaks. Proc. Natl. Acad. Sci. USA 105: 20876–20881.

Shakya, R., L. J. Reid, C. R. Reczek, F. Cole, D. Egli et al., 2011   BRCA1 tumor suppression depends on BRCT phosphoprotein binding, but not its E3 ligase activity. Science 334: 525–528.

Starita, L. M., J. N. Pruneda, R. S. Lo, D. M. Fowler, H. J. Kim et al., 2013   Activity-enhancing mutations in an E3 ubiquitin ligase identified by high-throughput mutagenesis. Proc. Natl. Acad. Sci. USA 110: E1263–E1272.

Tavtigian, S. V., A. M. Deffenbaugh, L. Yin, T. Judkins, T. Scholl et al., 2006   Comprehensive statistical study of 452 BRCA1 missense substitutions with classification of eight recurrent substitutions as neutral. J. Med. Genet. 43: 295–305.

Towler, W. I., J. Zhang, D. J. R. Ransburgh, A. E. Toland, C. Ishioka et al., 2013   Analysis of BRCA1 variants in double-strand break repair by homologous recombination and single-strand annealing. Hum. Mutat. 34: 439–445.

Vega, A., B. Campos, B. Bressac-De-Paillerets, P. M. Bond, N. Janin et al., 2001   The R71G BRCA1 is a founder Spanish mutation and leads to aberrant splicing of the transcript. Hum. Mutat. 17: 520–521.

Wu, W., K. Sato, A. Koike, H. Nishikawa, H. Koizumi et al., 2010   HERC2 is an E3 ligase that targets BRCA1 for degradation. Cancer Res. 70: 6384–6392.

Communicating editor: S. K. Sharan

GENETICS

Massively Parallel Functional Analysis of BRCA1 RING Domain Variants

Lea M. Starita, David L. Young, Muhtadi Islam, Jacob O. Kitzman, Justin Gullingsrud,
Ronald J. Hause, Douglas M. Fowler, Jeffrey D. Parvin, Jay Shendure, and Stanley Fields

Table S1 BRCA1 Variants

Amino acid change	HG19 Genomic Location	Category in manuscript	Notes	Reference
L30F	41267786G>T	cosmic		Forbes, S. A. et al. COSMIC: mining complete cancer genomes in the Catalogue of Somatic Mutations in Cancer. *Nucl. Acids Res.* **39**, D945-50 (2011).
L49M	41258539C>A	cosmic		Forbes, S. A. et al. COSMIC: mining complete cancer genomes in the Catalogue of Somatic Mutations in Cancer. *Nucl. Acids Res.* **39**, D945-50 (2011).
C47W	41258543C>G	cosmic		Forbes, S. A. et al. COSMIC: mining complete cancer genomes in the Catalogue of Somatic Mutations in Cancer. *Nucl. Acids Res.* **39**, D945-50 (2011).
C47R	41258545T>C	cosmic		Forbes, S. A. et al. COSMIC: mining complete cancer genomes in the Catalogue of Somatic Mutations in Cancer. *Nucl. Acids Res.* **39**, D945-50 (2011).
E9Q	41276088G>C	cosmic		Forbes, S. A. et al. COSMIC: mining complete cancer genomes in the Catalogue of Somatic Mutations in Cancer. *Nucl. Acids Res.* **39**, D945-50 (2011).
R7H	41276094C>T	evs	Less than 1% Allele Frequency	Exome Variant Server, NHLBI GO Exome Sequencing Project (ESP), Seattle, WA (URL: http://evs.gs.washington.edu/EVS/) [(October, 2014)].
G98C	41256894C>A	evs	Less than 1% Allele Frequency	Exome Variant Server, NHLBI GO Exome Sequencing Project (ESP), Seattle, WA (URL: http://evs.gs.washington.edu/EVS/) [(October, 2014)].
E23Q	41276047C>G	evs	Less than 1% Allele Frequency	Exome Variant Server, NHLBI GO Exome Sequencing Project (ESP), Seattle, WA (URL: http://evs.gs.washington.edu/EVS/) [(October, 2014)].
Q60R	41258506T>C	evs	Less than 1% Allele Frequency	Exome Variant Server, NHLBI GO Exome Sequencing Project (ESP), Seattle, WA (URL: http://evs.gs.washington.edu/EVS/) [(October, 2014)].
D67Y	41258486C>A	benign	IARC Class 1- Neutral	Easton, D. F. et al. A systematic genetic assessment of 1,433 sequence variants of unknown clinical significance in the BRCA1 and BRCA2 breast cancer-predisposition genes. *Amer. J. Hum. Gen.* **81**, 873-883 (2007).
R7C	41276095G>A	benign	benign	ClinVar – Sharing Clinical Reports Project
K45Q	41243060A>G	benign	IARC Class 1 – Not pathogenic	Easton, D. F. et al. A systematic genetic assessment of 1,433 sequence variants of unknown clinical significance in the BRCA1 and BRCA2 breast cancer-predisposition genes. *Am. J. Hum. Gen.* **81**, 873-883 (2007).
I68R	41258482A>C	VUS		ClinVar

Table S1 BRCA1 Variants

I68K	41258482A>T	VUS		ClinVar
D67E	41258484A>C	VUS		ClinVar
I89T	41256920A>G	VUS		ClinVar
I89M	41256919G>C	VUS		ClinVar
C39S	41267762A>T	pathogenic	Pathogenic (Clinical classification)	
K38N	41267763C>A	VUS		ClinVar
T69N	41258479G>T	VUS		ClinVar
T77M	41256956G>A	VUS		ClinVar
M18K	41276061A>T	VUS		ClinVar
M18T	41276061A>G	VUS	IARC Class 4 –likely pathogenic	Easton, D. F. et al. A systematic genetic assessment of 1,433 sequence variants of unknown clinical significance in the BRCA1 and BRCA2 breast cancer-predisposition genes. *Am. J. Hum. Gen.* **81**, 873-883 (2007).
L28P	41267794A>G	VUS		ClinVar
L49R	41258539A>C	VUS		ClinVar
I31M	41267784G>C	VUS		ClinVar
I21V	41276053T>C	VUS		ClinVar
C47G	41258546A>C	VUS		ClinVar
I42V	41267753T>C	VUS		ClinVar
I15L	41276071T>G	VUS		ClinVar
I15T	41276070A>G	VUS		ClinVar
E33Q	41267780C>G	VUS		ClinVar
L52F	41258531G>A	VUS		ClinVar
V11A	41276082A>G	VUS		ClinVar
T37R	41267767G>C	VUS		ClinVar
C24R	41276044A>G	VUS		ClinVar
C24Y	41276043C>T	VUS		ClinVar
D96N	41256900C>T	VUS		ClinVar
L63F	41258496T>A	VUS		ClinVar
K45N	41258550T>A	VUS		ClinVar
K45T	41267743T>G	VUS		ClinVar
G98R	41256894C>G	VUS		ClinVar
L87V	41256927A>C	VUS		ClinVar
S72R	41256970G>T	VUS		ClinVar
I90T	41256917A>G	VUS		ClinVar
H41R	41267755T>C	pathogenic	Pathogenic	Whiley, P. J. et al. Multifactorial likelihood assessment of BRCA1 and BRCA2 missense variants confirms that BRCA1:c.122A>G(p.His41Arg) is a pathogenic mutation. *PloS ONE* **9**, e86836 (2014)
C39R	41267762A>G	pathogenic	Pathogenic	ClinVar – Sharing Clinical Reports Project
C39Y	41267761C>T	pathogenic	IARC Class 5 – Definitely pathogenic	Sweet, K., Senter, L., Pilarski, R., Wei, L. & Toland, A. E. Characterization of BRCA1 ring finger variants of uncertain significance. *Br. Ca. Res. Treat.* **119**, 737-743 (2010).
R71G	41258474T>C	pathogenic	Pathogenic (causes aberrant splicing)	Vega, A. et al. The R71G BRCA1 is a founder Spanish mutation and leads to aberrant

Table S1 BRCA1 Variants

				splicing of the transcript. *Human Mutat.* **17**, 520-521 (2001).
R71K	41258473C>T	pathogenic	Pathogenic (causes aberrant splicing)	Zhang, L. et al. BRCA1 R71K missense mutation contributes to cancer predisposition by increasing alternative transcript levels. *Br. Ca. Res. Treat.* **130**, 1051-1056 (2011).
C61R	41258504A>G	pathogenic	Pathogenic	
C47F	41258545C>A	pathogenic	Pathogenic	
C64R	41258495A>G	pathogenic	Pathogenic	ClinVar – Sharing Clinical Reports Project
C64Y	41258494C>T	pathogenic	Pathogenic	ClinVar – Sharing Clinical Reports Project
C64G	41258495A>C	pathogenic	Pathogenic	ClinVar – Sharing Clinical Reports Project
L22S	41276049A>G	pathogenic	IARC Class 5 – Definitely	Sweet, K., Senter, L., Pilarski, R., Wei, L. & Toland, A. E. Characterization of BRCA1 ring finger variants of uncertain significance. *Br. Ca. Res. Treat.* **119**, 737-743 (2010).
T37K	41267767G>T	pathogenic	IARC Class 5 – Definitely	Sweet, K., Senter, L., Pilarski, R., Wei, L. & Toland, A. E. Characterization of BRCA1 ring finger variants of uncertain significance. *Br. Ca. Res. Treat.* **119**, 737-743 (2010).
C44S	41267747A>T	pathogenic	IARC Class 5 – Definitely	Sweet, K., Senter, L., Pilarski, R., Wei, L. & Toland, A. E. Characterization of BRCA1 ring finger variants of uncertain significance. *Br. Ca. Res. Treat.* **119**, 737-743 (2010).
C44Y	41267746C>T	pathogenic	IARC Class 5 – Definitely	Sweet, K., Senter, L., Pilarski, R., Wei, L. & Toland, A. E. Characterization of BRCA1 ring finger variants of uncertain significance. *Br. Ca. Res. Treat.* **119**, 737-743 (2010).
C44F	41267746C>A	pathogenic	Pathogenic	ClinVar – Sharing Clinical Reports Project
C61Y	41258503C>T	pathogenic	Pathogenic	ClinVar – Sharing Clinical Reports Project
C61G	41258504A>C	pathogenic	IARC Class 5 – Definitely	Spearman, A. D. et al. Clinically applicable models to characterize BRCA1 and BRCA2 variants of uncertain significance. *J. Clin. Oncol.* **26**, 5393-5400 (2008).

Table S2 is available for download as an Excel file at
www.genetics.org/lookup/suppl/doi:10.1534/genetics.115.175802/-/DC1
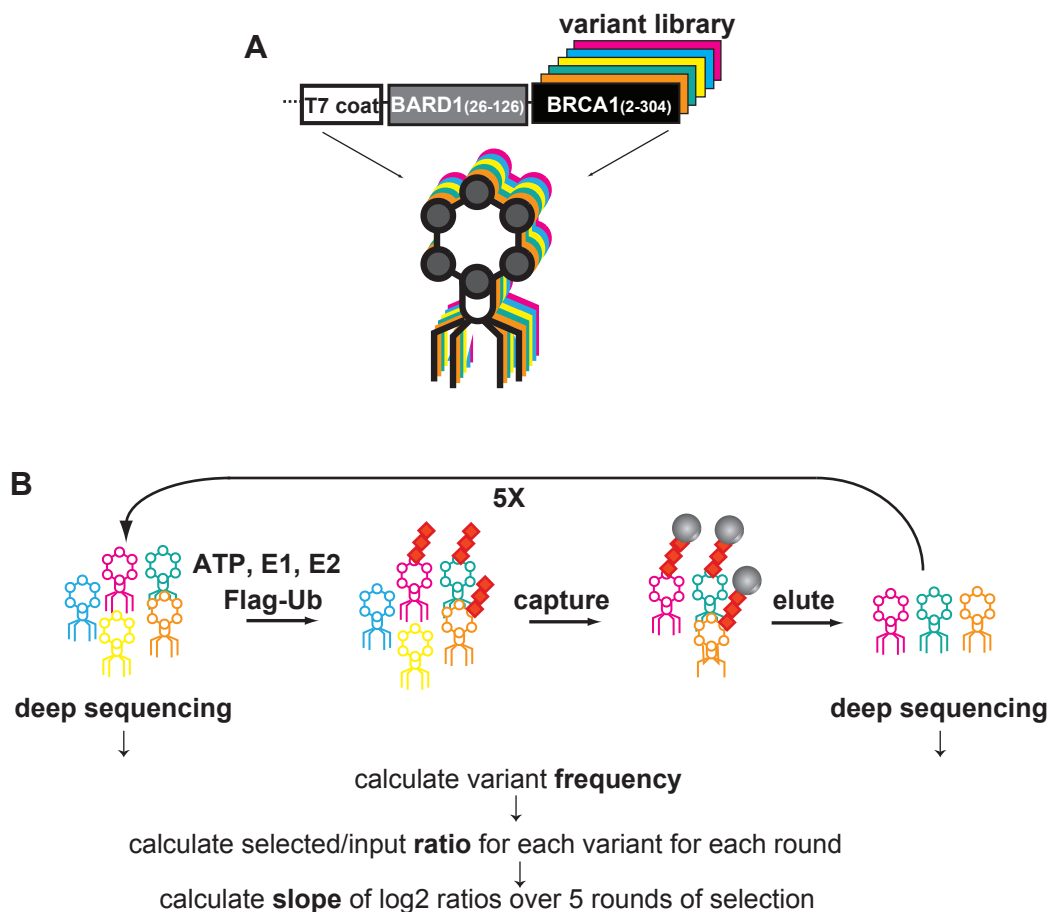
Table S3 Primers

Primer Name	Sequence
BRCA1_00284.0	tcgagtgcgggatctGAAAAGTATCAGGGTAGTTCTGTTTCAAAC TTGnnnGTGGAGCCATGTGGCACAAATACTagatcactgaggag a
JKR18	tctcctcagtgatct
JKL18	tcgagtgcgggatct
JKR18U	tctcctcagtgatcu
jkA0360_bbL8Lf	CGTTACAGTTCTGCGATTGATC agatggcggatccggcggc
jkA0306_bbLr	/5Phos/TTTATGCTTCCGGCTCGTAT
jkA0307x_bbRf	/5Phos/acgatctatccagattcatgcactactacagcatcagt AATTCTGGGGGAAGTGGTG
jkA0308x_bbRrbc	GGAAGAGCTCAAGGCAGGTC aagctt NNNNNNNNNNNNNNNNN TCATCTATTTA gaaCtcagccttttctacattca
L8	CGTTACAGTTCTGCGATTGATC
JKL18U	tcgagtgcgggatcu
W-E4B-subassembly-linker	CGGTCTCGGCATTCCTGCTGAACCGCTCTTCCGATCT
C-E4B-subassembly-linker	GATCGGAAGAGCGGTTCAGCAGGAATGCCGAGACCG
newBRCA1-side_F_CG1	AATGATACGGCGACCACCGAGATCTACACGCAGGCGGCCG CACTAGTGATccggAAGCTT
BRCA1-side_R_CG2	CAAGCAGAAGACGGCATACGAGATactgacacCGGTCTCGGC ATTCCTGCTGAACCGCTCTTCCGATCT
jkA0390_BBcplxcheckF	CTAAATGGCTGTGAGAGAGCTCAGaaggctgaGttcTAAATAG ATGA
E4B-index01_CG-R	CAAGCAGAAGACGGCATACGAGATAAAACCCCCCC AAG GGG TTA ACT AGT TAC TCG AGT GCG G
E4B-index02_CG-R	CAAGCAGAAGACGGCATACGAGATTTTTCCCCCCC AAG GGG TTA ACT AGT TAC TCG AGT GCG G
E4B-index03_CG-R	CAAGCAGAAGACGGCATACGAGATCCCCAAAACCC AAG GGG TTA ACT AGT TAC TCG AGT GCG G
E4B-index04_CG-R	CAAGCAGAAGACGGCATACGAGATGGGGAAAACCC AAG GGG TTA ACT AGT TAC TCG AGT GCG G
E4B-index05_CG-R	CAAGCAGAAGACGGCATACGAGATCACCACCACCC AAG GGG TTA ACT AGT TAC TCG AGT GCG G
E4B-index06_CG-R	CAAGCAGAAGACGGCATACGAGATGTGGTGGTCCC AAG GGG TTA ACT AGT TAC TCG AGT GCG G
E4B-index07_CG-R	CAAGCAGAAGACGGCATACGAGATTCATCATCCCC AAG GGG TTA ACT AGT TAC TCG AGT GCG G
E4B-index08_CG-R	CAAGCAGAAGACGGCATACGAGATACTGACTGCCC AAG GGG TTA ACT AGT TAC TCG AGT GCG G
JK19	AATGATACGGCGACCACCGAGATCTACACacgtaggcCTAAAT GGCTGTGAGAGAGCTCAG

Table S3 Primers

NexV2ad2_A1	CAAGCAGAAGACGGCATACGAGATTACGAAGTCGTCTCGT GGGCTCGGAGATGTGTATAAGAGACAG
SpeI_Gal4DBD_F	atcgatactagtgccgccaccatgaagctactgtcttctatcg
SpeI_Gal4DBD_R	tagaatactagtcgatacagtcaactgtctttg
EcoRI_BARD_Ln_F	atcgtcgaattcggggggaagtggtgg
NcoI_BARD_Stop_R	tgacgtccatggctaatcttctttcaaatctgacagc
BRCA1-Y2H_commonLinker_R	GTCTCGTGGGCTCGGAGATGTGTATAAGAGACAGATGGGA TGTGCTGCAAGGCGATTAAG

Figure S1 Construction of the BRCA1(2-304) allelic series.
(A) We created an allelic series of variants within BRCA1(2-304) with single amino acid substitutions by the method known as Programmed Allelic Series (Kitzman et al. 2015), which uses mutagenic oligonucleotides synthesized on a programmed microarray to create a pool of variants with single codon changes by overlap-extension PCR. **(B)** Each variant was barcoded with a random 16-nucleotide tag that we associated with the mutation present in the BRCA1 domain. We assembled 128,237 barcoded variants, of which 60,256 corresponded to 5,156 single amino acid changes out of the possible 5,757 (89% of the 19 substitutions x 303 codons) in BRCA1(2-304). **(C)** The number of barcodes per assembled BRCA1(2-304) variant is represented in a heatmap. Shades of blue represent the number of barcodes per variant with the maximum color fill set to 25 barcodes. There were many variants that had more than 25 barcodes. Yellow represents wild-type residues and gray potential variants for which there was not a full length BRCA1(2-304) assembly.
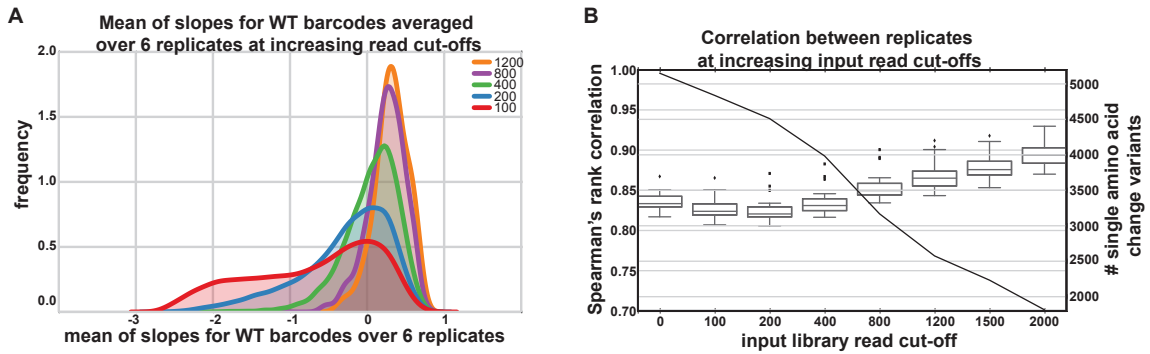
Figure S2 Scoring the effects of missense mutation on the E3 ligase activity of the BRCA1 RING domain.

(A) A fusion protein of BARD1(26-126) and BRCA1(2-304) is an active E3 ligase and capable of autoubiquitination in vitro. The allelic series of BARD1(26-126) - BRCA1(2-304) was expressed at the carboxy-terminus of the coat protein of bacteriophage T7. Residues 2-103 are the structured RING domain and lysine residues within 104-304 are required for autoubiquitination.

(B) A phage population displaying the library of BRCA1 variants was incubated in ubiquitination reactions (purified E1, E2 (UbcH5c), Flag-tagged ubiquitin and ATP), in triplicate in two separate experiments. Phages encoding active variants of BRCA1 became ubiquitinated and were collected on anti-Flag beads. After washing, elution by competition with Flag peptide and re-amplification in E. coli, phages were used in the next round of selection. Phage DNA was extracted after each of five sequential rounds of selection and the barcodes were amplified by PCR and sequenced. Barcodes were tallied by single end Illumina sequencing. After converting the barcodes to BRCA1(2-304) variants, we calculated the frequency of each variant in the input and selected populations. For each of the five rounds of selection, we fit a linear curve to the log ratio of the frequency of each variant divided by its frequency in the input population for each of the six replicates. The functional score for each variant is the slope of the fit curve, normalized by setting stop codons to a score of 0 and the wild-type to a score of 1.

A Mean of slopes for WT barcodes averaged over 6 replicates at increasing read cut-offs

B Correlation between replicates at increasing input read cut-offs

Figure S3 Heuristic for filtering high-confidence data set.
(A) The distribution of the log transformed slopes of the nearly 30,000 barcodes (Figure S1) associated with wild-type BRCA1(2-304) sequences (input read cut-offs represented by color). The poor scoring wild-type variants are thought to be due to loss of individual barcodes that follows a Poisson distribution due to experimental bottlenecks. **(B)** The 800 input read count cut-off maximizes the number of variants contributing to the analysis (black line) while maintaining the maximum Spearman's rank correlation between the six experimental replicates and minimizing barcode dropout due to bottlenecks (A). Estimates of variance and 95% confidence intervals can be found for each measurement in Table S2.
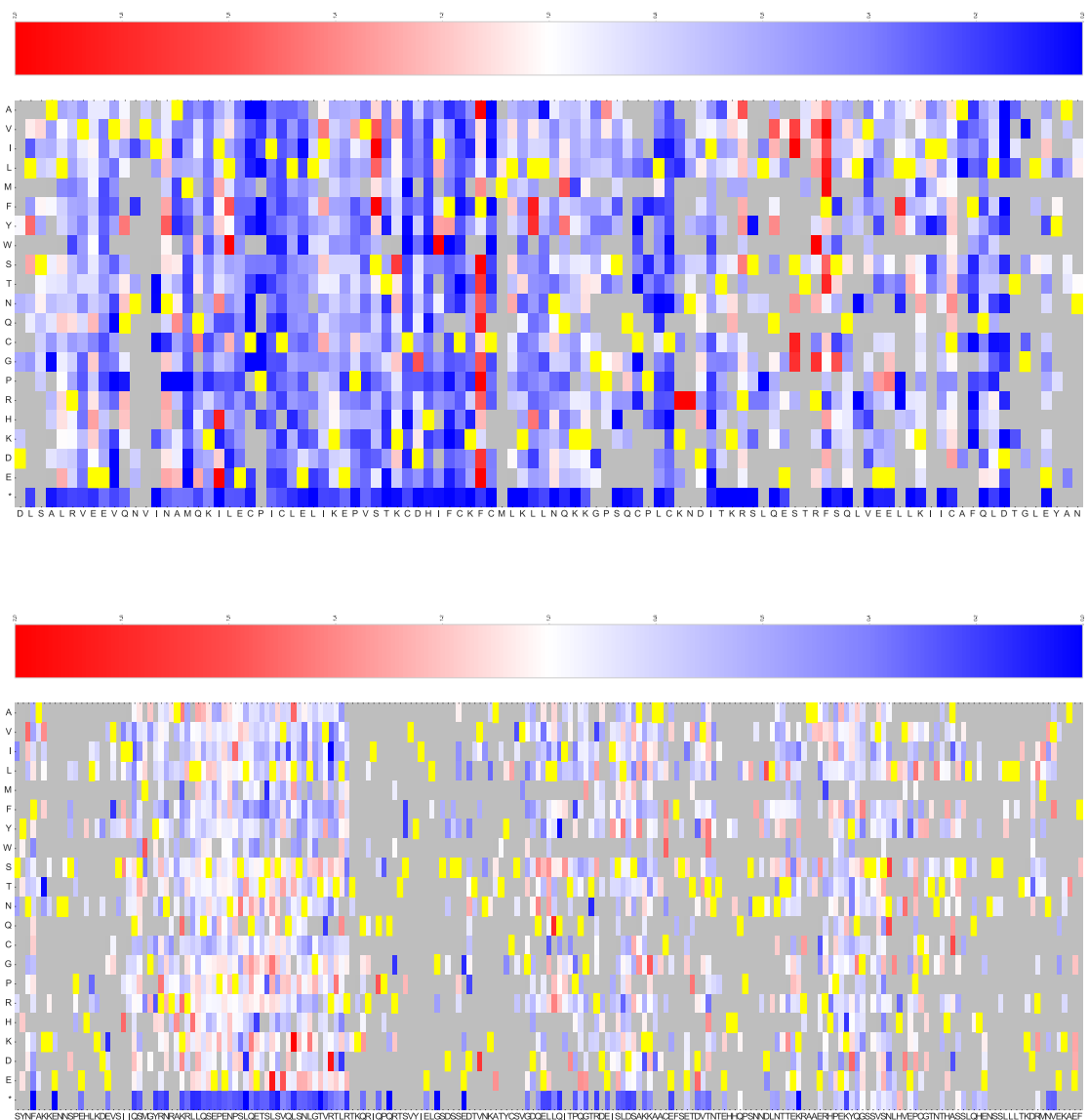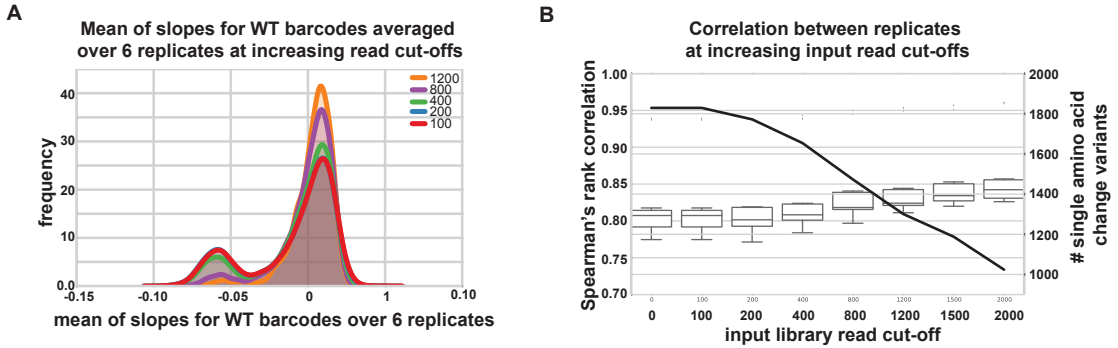
Figure S4. Sequence - function map of the effect of missense substitutions on E3 ligase function. The functional score for each variant is the slope of the fit curve, normalized by setting stop codons to a score of 0 and the wild-type to a score of 1. Each position in BRCA1(2-304) is arranged along the x-axes. The amino acid substitutions, grouped by side-chain properties, are on the y-axes. The E3 ligase scores range from improved activity versus wild-type (red), equivalent to wild-type (white), to less than wild-type (blue). Yellow represents the wild-type residue and gray missing or low confidence data.
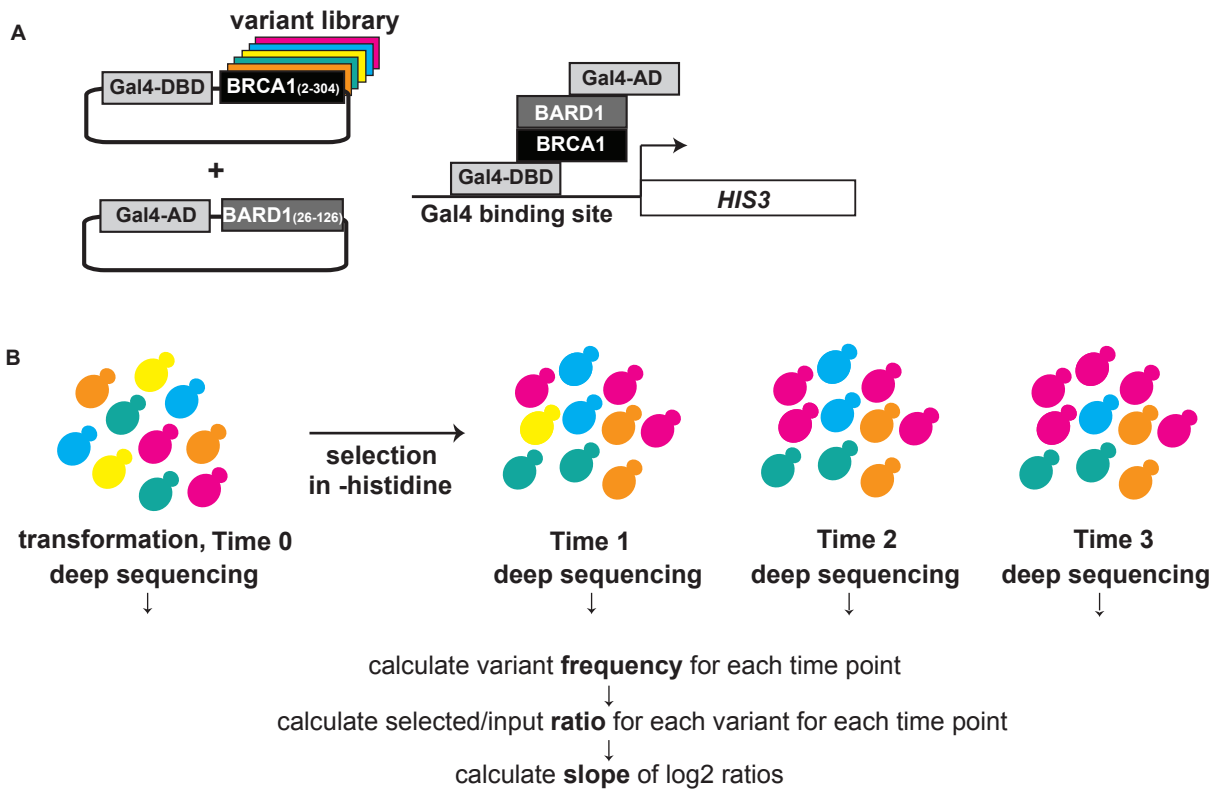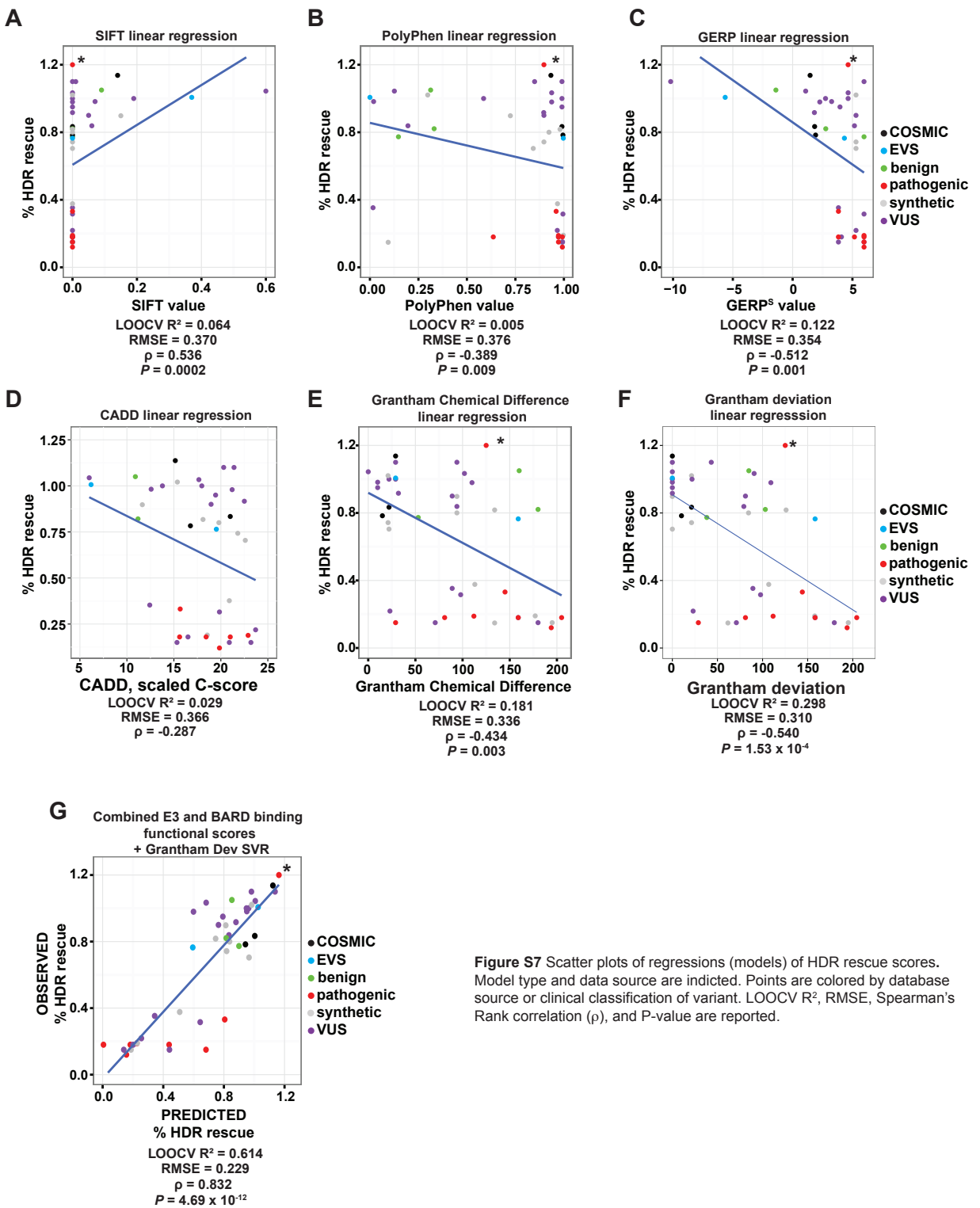
Figure S5 Diagram of the yeast-two-hybrid selection scheme to measure BRCA1-BARD1 binding.
(A) The barcoded allelic series of BRCA1(2-304) was fused to the carboxy-terminus of the Gal4 DNA-binding domain, and the BARD1(26-126) domain was fused to the carboxy-terminus of the Gal4 activation domain. Yeast harboring BRCA1 variants that bind to BARD1 drive the expression of the HIS3 reporter gene and therefore grow in media lacking histidine. **(B)** The two-hybrid reporter strain transformed with the plasmids encoding the BRCA1 allelic series and BARD1 was selected in triplicate in two separate experiments in media lacking histidine and containing 10 mM 3-amino-1,2,4-triazole (3-AT), a competitive inhibitor of the His3 enzyme. At mid-log phase, aliquots of the cultures were sampled and then back-diluted into fresh selective media and grown to mid-log phase two additional times. The BRCA1 plasmids were extracted at each of three time points and their barcodes were PCR amplified and sequenced. The barcodes associated with BRCA1(2-304) plasmids prepped from the yeast after each of the three time points of selection and the input population were deeply sequenced. We fit a linear curve to the log ratio of the frequency of each variant in the selected populations divided by its frequency in the input population and calculated the slope of that line, normalized again to stop codons (set to 0) and wild-type (set to 1).

A

Mean of slopes for WT barcodes averaged over 6 replicates at increasing read cut-offs

B

Correlation between replicates at increasing input read cut-offs

Figure S6 Heuristic for filtering high-confidence data set.
(A) The distribution of the log transformed slopes of the nearly 30,000 barcodes (Figure S1) associated with wild-type BRCA1(2-304) sequences (input read cut-offs represented by color). The poor scoring wild-type variants are thought to be due to loss of individual barcodes that follows a Poisson distribution due to experimental bottlenecks. **(B)** The 800 input read count cut-off maximizes the number of variants contributing to the analysis (black line) while maintaining the maximum Spearman's rank correlation between the six experimental replicates and minimizing barcode dropout due to bottlenecks (A). Estimates of variance and 95% confidence intervals can be found for each measurement in Table S2.

Figure S7 Scatter plots of regressions (models) of HDR rescue scores. Model type and data source are indicted. Points are colored by database source or clinical classification of variant. LOOCV R^2, RMSE, Spearman's Rank correlation (ρ), and P-value are reported.